

Tensile Properties of Forged Direct-Squeeze-Cast Al-(6.0~8.0 mass%)Si-(0.3~0.52 mass%)Mg Alloy

Teng-Shih Shih, Po-Chen Chen* and Wei-Shian Tsai*

National Central University, Department of Mechanical Engineering Chung-Li, Taiwan 32001, R. O. China

The effects of lubricants on the quality of squeeze-cast Al-(6.0~8.0 mass%)Si-(0.3~0.52 mass%)Mg alloys were studied. Different melts with varying amounts of Si and Mg were prepared and then directly squeeze-cast into cakes. Different lubricants and two different pressures, 60 and 120 MPa, were used in the production of the cakes. These squeeze-cast cakes were then forged and heat-treated. Tensile specimens prepared from the forged and heat-treated cakes were tested to determine their tensile properties. Among all the variables tested, the Weibull modulus (in ultimate tensile strength, UTS) was the largest ($m = 53.7$) for the cakes squeeze-cast at 120 MPa using water-based BN powder ($\sim 4 \mu\text{m}$ in size) as a lubricant. After polishing and ultrasonic-vibration treatment, oxide films appeared as foggy films on the chilled blocks and forged cakes. Reaction films were also observed on the tensile fracture surfaces of the tested bars. They were particularly apparent on the bars produced from cakes that had been prepared using an oil-based lubricant. The area ratios of the foggy films and reaction films on the samples were calculated. The Weibull modulus (in UTS) of the forged cakes after T6 treatment was significantly affected by both the pore count and the total area ratio covered by reaction films and foggy films. [doi:10.2320/matertrans.MRA2007132]

(Received June 22, 2007; Accepted January 10, 2008; Published March 25, 2008)

Keywords: A356 alloy, direct squeeze-casting, pore counts, foggy films

1. Introduction

The A356 alloy is widely used in industry due to its superior fluidity during casting as well as the good corrosion resistance and mechanical properties of the final product. Moreover, precipitation treatment can greatly improve the mechanical properties of A356 castings. The strength of this alloy is mainly due to the uniform precipitation of Mg_2Si dispersed in the matrix. According to the specification of the AA standard, the A356 alloy contains 6.5 to 7.5 mass% Si and 0.25 to 0.45 mass% Mg. The mechanical properties and fluidity of Al-Si alloys are significantly affected by their silicon content over a practical range of 5~16 mass%.^{1,2)} Increasing the silicon content increases the latent heat released during solidification, and hence, greatly improves the fluidity and feedability of the solidified liquid, thus reducing shrinkage.³⁾ An increase of 0.1 mass% in the Mg content yields an increase of about 70 MPa in the T6 yield strength for a Mg content between 0.05 and 0.5 mass%.⁴⁾ Increasing the Mg content from 0.3 to 0.5 mass% has a minor effect on the hydrogen pick-up of the A380 alloy melt, but increases the total amount of Mg-bearing inclusions.⁵⁾

The squeeze-casting process is characterized by good heat transfer during solidification. This implies that both the grain size and/or dendrite arm spacing in the as-cast structure are sufficiently fine.^{6,7)} Squeeze-cast AC4CH alloys (which have properties similar to the A356 alloy) have both high tensile strength (273 MPa) and increased elongation (21%). This occurs because of their fine, spherical eutectic Si particles and small dendrite arm spacing.⁸⁾ Shih *et al.* studied the effects of Si and Mg on the mechanical properties of indirect-squeeze-cast Al-(6.5~11 mass%) Si-(0.3~0.5 mass%) Mg alloys.⁹⁾ T6-treated Al-7Si-0.3Mg alloys were found to have an ultimate tensile strength (UTS) of 269 MPa and an elongation of 12.7%; the values for T6-treated gravity castings were 221 MPa and 4.7%, respectively. The UTS

values of different castings were also compared, and the results showed that squeeze-casting yields a better UTS than gravity casting.

During squeeze-casting, the pressure should be sufficiently low so that segregation does not occur, but sufficiently high to prevent shrinkage.¹⁰⁾ Hong *et al.* developed an empirical equation to predict the soundness of the casting as well as the occurrence of macrosegregation and shrinkage defects in directly squeezed Al-7 Si alloy castings.¹¹⁾ They suggested that sound castings could be obtained when the applied pressure (P) satisfies $P_{\text{SC}} < P < P_{\text{MS}}$, where P_{SC} is the critical applied pressure below which shrinkage defects occur, and P_{MS} is the critical applied pressure above which macrosegregation occurs. In this study, the applied pressure, die temperature, and pouring temperature were 60 MPa, 473 K, and 993 K, respectively; using these values, sound alloy cakes could be produced, as described by Hong *et al.*¹¹⁾ These cakes were then forged to the specified thickness. The tensile properties of the bars thus prepared were then evaluated.

2. Experimental Procedure

Different melts (25 kg) were prepared using an induction furnace with a clay-graphite SiC crucible. Two melts were prepared by melting commercially available A356 alloy ingots (MM samples); this set of samples had an intermediate Si and Mg content. Four other sets of samples were prepared from commercial A356 alloy ingots, pure Al, and master alloys of Al-20%Si and pure Mg. These samples were divided into two groups according to their Si and Mg contents: samples with high silicon and high magnesium contents (HH samples), and those with low silicon and low magnesium contents (LL samples). Table 1 shows the chemical compositions of the six sets of samples. The melts were held at 993 K and degassed for 900 s using nitrogen and a degassing diffuser. After degassing, the melts were held at 993 K for 900 s. Some of the melts were then poured into a

*Graduate Student, National Central University

Table 1 Chemical analysis of six sets of samples where LL indicates low Si and low Mg content; MM and HH represents intermediate and high Si and Mg content; the squeezing pressure is 60 and 120 MPa; the MM sample was prepared from commercial A356 ingots.

Mass%	Si	Mg	Fe	Ti	Sr (ppm)	Al
Alloy						
HH 60	7.64	0.52	0.07	0.08	22	Balance
HH 120	8	0.48	0.06	0.08	17	Balance
LL 60	6	0.30	0.07	0.07	11	Balance
LL 120	6	0.30	0.06	0.07	13	Balance
MM 60	7.27	0.35	0.06	0.16	15	Balance
MM 120	7.54	0.39	0.06	0.12	11	Balance

HH: high silicon and magnesium contents (from A356 ingot and master alloy).

MM: intermediate silicon and magnesium contents (from commercial A356 ingot).

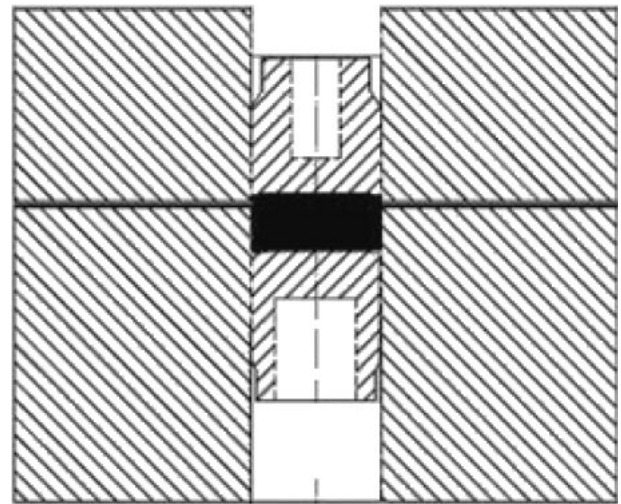
LL: low silicon and magnesium contents (from A356 ingot and master alloy). 60 and 120 represent the squeezing pressure in MPa.

die to produce chilled blocks 50 mm in diameter and 20–25 mm in thickness, while other melts were used to produce squeeze-cast cakes (80 mm in diameter and 25~30 mm in thickness) at two pressures: 60 and 120 MPa. Samples from the chilled blocks were polished and then analyzed using a chemical spectrometer.

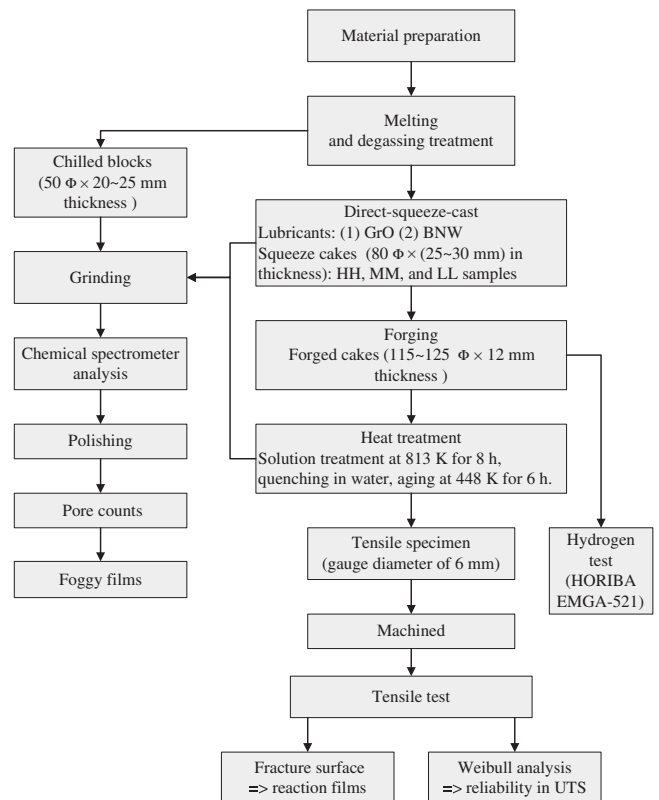
For the squeeze-casting, types of lubricants were prepared: graphite (Gr: 10~40 μm) powder as an oil-based lubricant (GrO), and BN (~4 μm) powder as a water-based lubricant (BNW). The GrO lubricant was brushed onto the cavity wall, and the plunger surface of the die was sprayed uniformly using compressed air. The BNW lubricant was sprayed using a nozzle and high-pressure compressed air in order to uniformly coat the cavity wall and plunger surface. A vertical-type 500-ton hydraulic press was used to produce the direct-squeeze-cast cakes. Figure 1(a) shows a schematic illustration of the die set along with the squeeze-cast cakes in the die cavity. In preparation for pouring, the die was preheated to $463 \pm 10 \text{ K}$ and the melt was held at $1003 \pm 5 \text{ K}$. First, the lubricant was sprayed into the die cavity, and then the melt was poured in. Next, the upper and lower parts of the die were closed and the lower part or plunger was forced upward to apply a pressure of 60 or 120 MPa on the molten metal. The molten metal was squeezed for about 10 s to produce a cake 80 mm in diameter and 25~30 mm in thickness. The cakes were removed, heated (673 K), and then forged on a flat open die to a thickness of 12 mm; the samples were deformed to a true strain of about 0.45~0.55. The forged samples were heat-treated at 813 K for 8 h (solution treatment) and then quenched in water prior to aging at 448 K for 6 h. After the heat-treatment, six tensile bars with a gauge diameter of 6 mm were machined from each cake. Sets of 18–20 tensile bars were prepared for tensile tests.

After tensile testing, the Weibull distribution was utilized to construct a plot of $\ln\{\ln[1/(1 - Fw)]\}$ versus UTS for each set of data, where Fw indicates the cumulative fraction of failure during tensile testing. The slope of this plot is termed as the Weibull modulus. Specimens with a high modulus are strong and reliable in terms of their UTS.¹²⁾

The chilled blocks, squeeze-cast cakes, and forged cakes were sectioned into two halves, one of which was polished.



(a)



(b)

Fig. 1 (a) Schematic illustration of the die set for making direct-squeeze-cast cakes, including the lower die, lower plunger, upper die, and upper plunger. (b) Flowchart describing the entire experimental procedure.

The pore count was measured under 100X and 500X magnifications at ten locations and the average pore count with its standard deviation was obtained. The other halves of the chilled blocks, squeeze-cast cakes, and forged cakes were also polished and then subjected to ultrasonic-vibration treatment in order to determine the area ratio of the foggy films (or foggy marks).¹³⁾

The fracture surfaces of the tensile bars were observed (5~20X magnification). The numbers of film-like marks (brown or black in color) were counted and the area fractions were recorded. Reaction films can be distinguished as foggy

films that appear on the surface of a polished sample after it has been subjected to ultrasonic-vibration treatment. Figure 1(b) shows a flowchart of the procedure, describing the sample preparation, pore counts, measurement of foggy films and reaction films, mechanical testing, and Weibull analysis.

3. Results and Discussion

3.1 As-cast and forged-plus-heat-treated microstructures

After pouring the molten metal into the die cavity, the upper and lower parts of the die were closed. The pouring time was about 2~3 s. The plunger was moved upward to squeeze the molten metal against the upper plunger. The molten metal in the cavity was thus squeezed and solidified under a pressure of 60 or 120 MPa. The heat was transferred from the solidifying metal to the mold as the casting cooled.⁶⁾ The solidification occurred at a high cooling rate, which caused the formation of fine dendrites near the surface, especially in areas close to the lower plunger. Figure 2 shows the microstructure of the as-cast A356 cakes under 60 MPa. The areas marked 2, 4, and 6, which were close to the lower plunger, show typical, fine α -Al dendrites. The areas marked 1, 3, and 5 show a higher eutectic fraction than those marked 2, 4, and 6 near the lower plunger. During solidification, a fine dendritic structure tends to develop near the die wall in squeezed molten metals, where heterogeneous nucleation and rapid cooling dominate the solidification. The formation of a layer of fine α -Al dendrites reduces the effectiveness of heat extraction from the remaining molten metal. This is because the surface contraction of the solidified skin decreases the heat transfer coefficient at the interface. However, as the squeezing pressure continues to push the remaining molten metal, it sometimes causes the solidified α -Al dendrites to break. As a result, the molten metal penetrates into the areas near the surface layer, correspondingly increasing the eutectic fraction. This is particularly apparent at the corners of the squeeze-cast cakes; see location 5 in Fig. 2. The central areas of the squeeze-cast cakes were macroscopically sound, as seen at locations 7 and 8.

When the pressure was increased from 60 to 120 MPa, the eutectic fractions increased slightly at locations 7 and 8 in Fig. 2. The increased pressure is expected to enhance the heat transfer from the solidified metal near the die wall. The fraction of the α -Al phase increased in the area near the die wall, raising the solute content in the remaining liquid. Thus, the central areas of the squeeze-cast cakes possessed a greater eutectic fraction when subjected to a higher pressure of 120 MPa. The squeeze-cast cakes were macroscopically sound when the pressure was either 60 or 120 MPa. Microscopic observation showed that the eutectic Si particles had been well modified to a fibrous morphology due to a rapid cooling rate of 25~40 K/s.

Figure 3 shows the structure at different locations in the forged cakes after T6 treatment. The matrix was heavily deformed and exhibited elongated grains (or subgrains) aligned in the direction of deformation. Macroscopically, the deformed structures were uniformly distributed throughout the matrix in the forged cakes. We can compare the structures

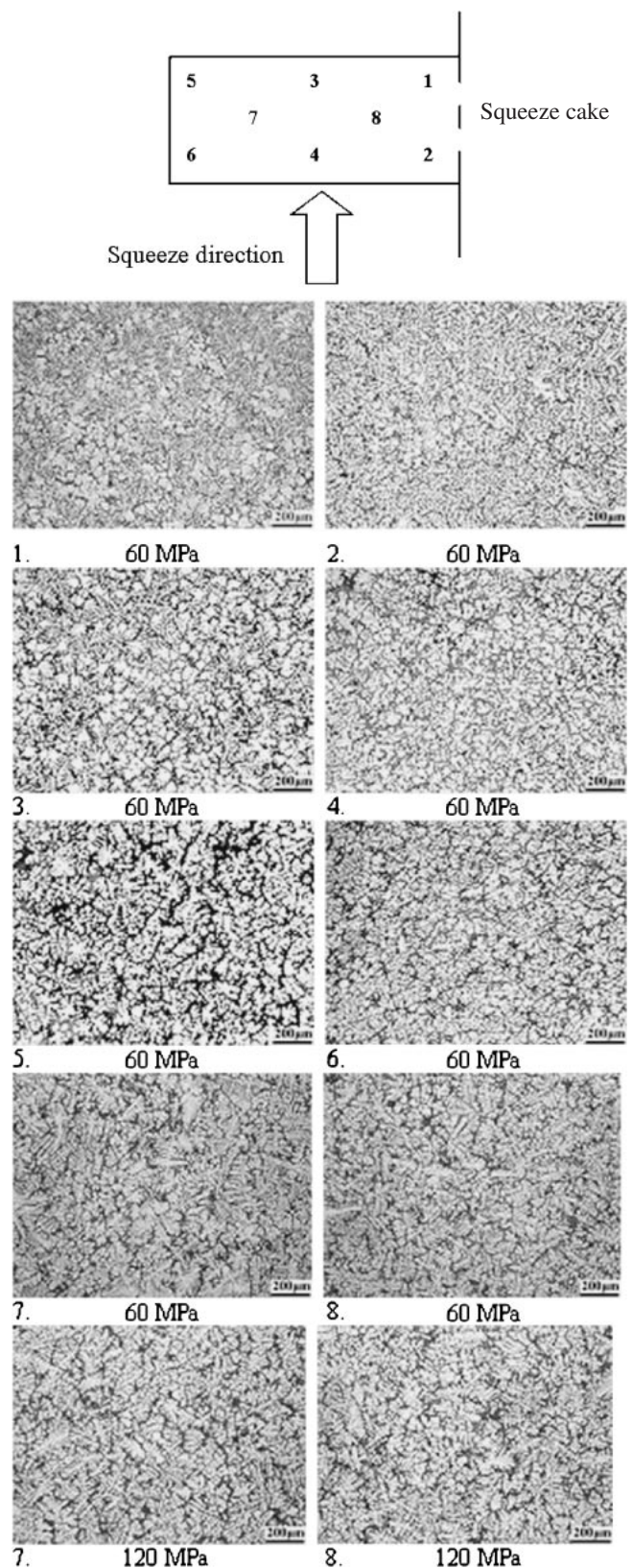


Fig. 2 Microstructure of a direct-squeeze-cast cake: locations 1, 3, and 5 are near upper plunger; locations 2, 4, and 6, near the lower plunger; and locations 7 and 8, at the center of the cakes. Samples were produced with GrO lubricant, squeezing pressure of 60 and 120 MPa, mold temperature of 463 ± 10 K, and pouring temperature of 1003 ± 5 K.

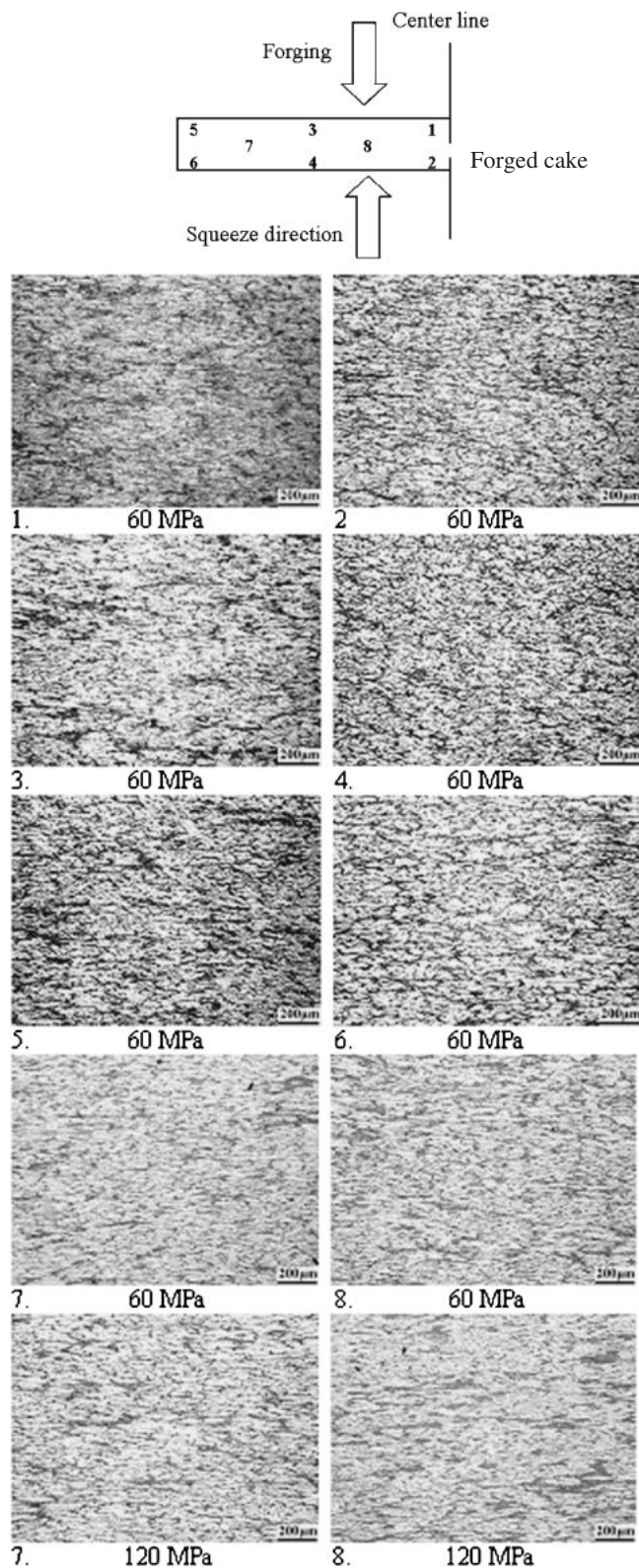


Fig. 3 Microstructure of the forged cakes after T6 treatment of the direct-squeeze-cast cakes shown in Fig. 2; T6 treatment: 813 K for 8 h and 448 K for 6 h.

at different locations in Fig. 3 with the corresponding areas in Fig. 2.

3.2 Foggy films and pore count

Figure 4 shows the foggy films recorded on different

samples after ultrasonic-vibration treatment; also see Table 2. The foggy films covered a larger surface area on the chilled blocks than on either the squeeze-cast or forged samples. The squeeze-cast cakes were subjected to a high pressure of 60 or 120 MPa during solidification. As mentioned, the squeezing of the solidified skin of the melt near the die wall might possibly have lead to the breaking of the dendrites trapped in the oxide film. The oxide films were broken into pieces. The fragmented oxide films could be further decreased by forging, as shown in Fig. 4. Table 2 shows area ratios of foggy films: 2.5~5.8% for chilled blocks and 0.7~2.2% for squeeze-cast cakes. On the forged cakes, the foggy films were further decreased to 0.4~0.6%.

These foggy films have been identified as oxide films with varying oxygen contents.¹⁴⁾ These entrapped oxide films are fragile; hence, when they are subjected to deformation strain, cracks tend to be initiated within them.¹⁴⁻¹⁶⁾ Therefore, it is beneficial to decrease the area ratios of foggy films in order to decrease the number of crack initiation sites.

Before being subjected to ultrasonic-vibration treatment, all the samples were observed under an optical microscope to record the pore counts under different magnifications (100X and 500X). Scanning electron microscopy (SEM) was also used to identify the pores. We found fine Si particles, mostly $\leq 1 \mu\text{m}$ in size; while the micropores were $1\sim 3 \mu\text{m}$ in size and mostly free of trapped particles. The entrapped BN particles were in the size range of $3\sim 5 \mu\text{m}$, while the entrapped Gr particles had sizes varying from 3 to $28 \mu\text{m}$, depending on the location and degree of deformation to which the samples were subjected. Next, we discuss the effects of the pore count and pore size ($\geq 5 \mu\text{m}$) on the UTS.

The measured pore counts ($\geq 5 \mu\text{m}$) for different samples are listed in Table 2. The pore counts for the chilled blocks were higher ($92\sim 102 \text{ counts/mm}^2$), which decreased remarkably to $47\sim 69 \text{ counts/mm}^2$ in the squeeze-cast cakes; furthermore, the pore counts for the forged cakes were close to those for the squeeze-cast cakes ($49\sim 72 \text{ counts/mm}^2$). The fraction of pores that were $5\sim 10 \mu\text{m}$ in size was about 0.55–0.65, while that of pores greater than $20 \mu\text{m}$ in size was less than 0.1. The Gr or BN powders in the lubricants were entrapped in the poured metal and pressed during the casting and forging processes. The Gr particles collapsed; this caused an increase in the fraction of large pores: $15\sim 28 \mu\text{m}$ in Fig. 5. However, the use of the finer BN powder could increase the fraction of finer pores ($5 \mu\text{m}$).

3.3 Mechanical properties

Table 2 lists the tested mechanical properties and the recorded pore counts and area ratios of foggy films and reaction films for the different sets of samples. Figure 6 shows the plots of $\ln[\ln\{1/(1 - Fw)\}]$ versus $\ln \text{UTS}$ for six sets of data. The Weibull modulus (m) for the different sets of samples was also included. Increasing the Si and Mg contents increased the UTS ($283\sim 286$ versus $271\sim 276 \text{ MPa}$), as can be seen by comparing the results for HH60 and HH120 with those for LL60 and LL120. However, keeping the Si and Mg low (two sets of LL samples) was beneficial for developing stable elongation: 12.3% and 12.5% (with low deviations of 1.0% and 2.0% for the LL samples, respectively) as compared with 12.6% and 11.8% (with deviations of 2.4%

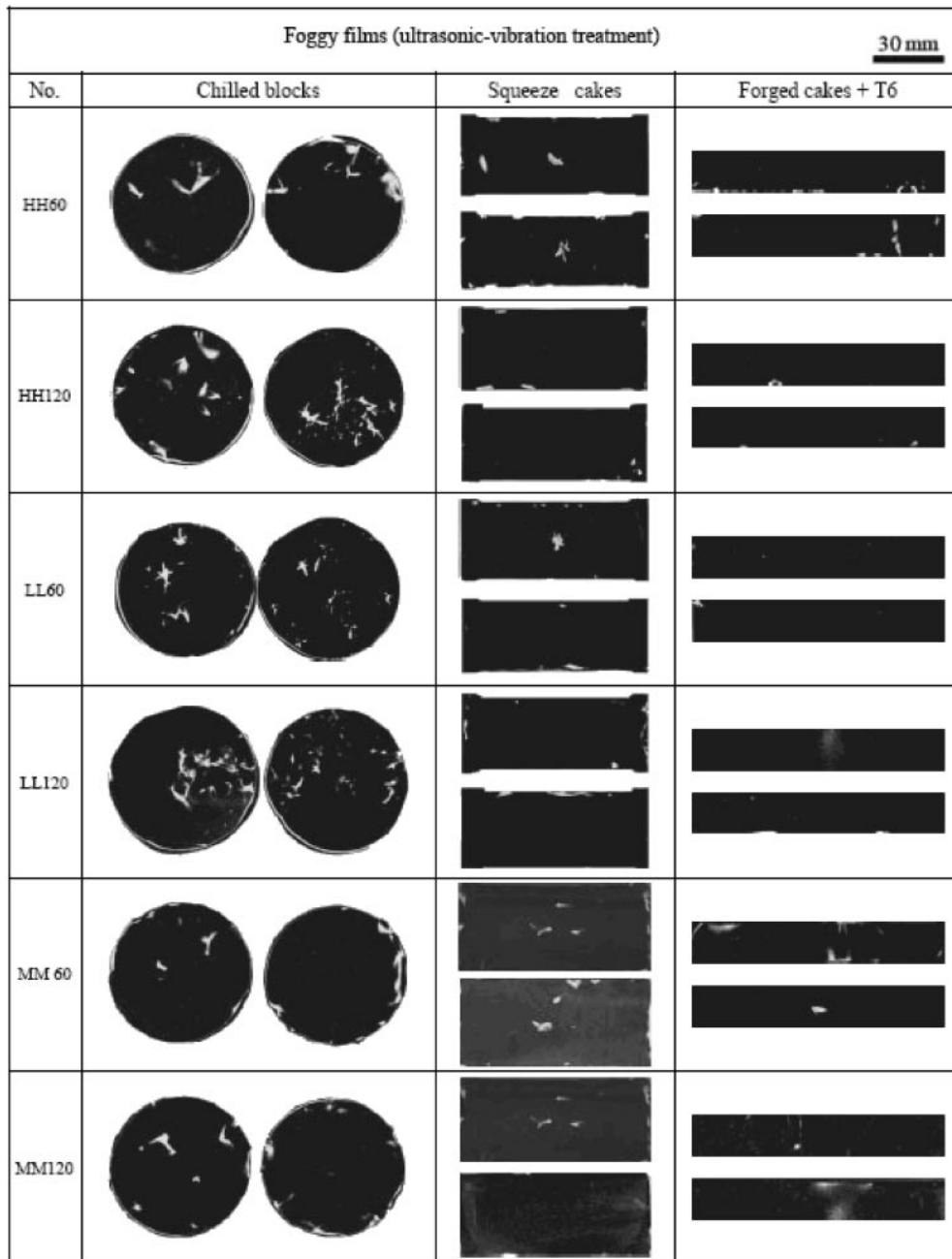


Fig. 4 Foggy marks recorded on the different samples, including the chilled blocks, squeeze-cast cakes, and forged (after T6 treatment) cakes.

and 1.9%, respectively) for the HH samples (see Table 2). The first four sets of data are for the squeeze-cast cakes produced using the BNW lubricant, while the other two sets (MM) are for those produced using the GrO lubricant. The set of samples produced with low Si (6%) and Mg (0.3%) contents using the BNW lubricant possessed a high Weibull modulus of 53.7.

The area ratios of reaction films were significantly affected by the lubricant used. The reaction films on the GrO samples covered an area almost 4~5 times larger than that on the BNW samples. Figures 7(a) and 7(b) show the fracture surfaces of samples HH60 and LL60, and Figs. 7(c) and 7(d) show those of samples MM60 and MM120. The former samples were produced using lubricant BNW and show 0.28% and 0.23% coverage by reaction films. The latter

samples were produced using lubricant GrO and show 1.01% and 0.84% coverage by reaction films.

Figures 8(a) and 8(b) show the relation of the pore counts (counts/mm²) and area ratios of the foggy films plus reaction films (FRFs) with the Weibull modulus (in UTS) for the six sample sets. Reaction films entrapped in the matrix (discussed later) could be traced to the reaction products that were produced between the molten metal and lubricant during pouring, while the foggy films indicated entrapped oxide films. They are both considered as part of the area ratio and lead to deterioration in the tensile properties of the samples. Therefore, the effect of film-type defects on the tensile properties of samples was correlated with the area ratio of foggy films and reaction films; these were added together to make up a single factor. The MM120 samples had

Table 2 Tested UTS, YS and elongation associated with measured pore counts and area ratios of foggy marks, reaction marks on chilled blocks, squeeze-cast cakes, forged cakes after T6 treatment, including the six sets of samples listed in Table 1.

Property Sample	Composition mass%	UTS MPa	Y.S. MPa	E. % (STDEV)	Weibull modulus	Foggy films, % (*)			Reaction films, % (**)		FRFs, %	Pore counts, (counts/mm ²) (***)			Hydrogen, cc/100 g (****)
						Chilled blocks	Squeeze- cast cakes	Forged cakes + T6	Tensile bar	Chilled blocks		Squeeze-cast cakes	Forged cakes + T6	Forged cakes	
HH60	Si: 7.64 Mg:0.52	285.8	118.0	12.6 (2.4)	9.9	5.3 (1.2)	2.2 (0.9)	0.6 (0.3)	0.28 (0.18)	2.48	102.1 (16.1)	68.7 (15.7)	71.9 (17.3)	0.30 (0.02)	
HH120	Si: 8.00 Mg:0.48	282.9	148.2	11.8 (1.9)	14.3	5.8 (1.6)	1.1 (2.1)	0.6 (0.2)	0.26 (0.16)	1.36	95.0 (14.6)	64.8 (15.4)	61.6 (15.6)	0.29 (0.07)	
LL60	Si: 6.00 Mg:0.30	270.5	119.3	12.3 (1.0)	27.3	3.0 (0.2)	0.9 (0.4)	0.5 (0.1)	0.23 (0.15)	1.13	102.1 (16.4)	51.3 (13.2)	52.0 (13.2)	0.22 (0.03)	
LL120	Si: 6.00 Mg:0.30	276.4	138.5	12.5 (2.0)	53.7	4.2 (1.5)	0.7 (0.5)	0.6 (0.2)	0.18 (0.13)	0.88	95.6 (16.7)	46.8 (11.7)	48.8 (12.1)	0.27 (0.02)	
MM 60	Si: 7.27 Mg:0.35	269.9	149.8	16.3 (3.3)	6.7	2.7 (1.3)	1.2 (0.3)	0.4 (0.2)	1.01 (1.64)	2.21	95.6 (16.6)	50.7 (11.3)	50.7 (11.8)	0.32 (0.05)	
MM 120	Si: 7.54 Mg:0.39	281.6	154.9	12.4 (1.3)	25.5	2.5 (0.1)	0.8 (0.7)	0.4 (0.3)	0.84 (1.56)	1.64	92.4 (15.2)	56.5 (14.6)	55.8 (11.4)	0.31 (0.03)	

(*) Standard deviation for 2 tests.

(**) Standard deviation for 20 tests; measured from fracture surfaces of tensile bars.

(***) Standard deviation for 10 tests; particle & pore counts.

(****) Standard deviation for 3 tests for samples taken from tensile bars; the hydrogen analyzer (cc/100 g Al) used was a HORIBA EMGA-521.

FRFs: sum of area ratios of reaction films on tensile bars and foggy films on squeeze-cast cakes.

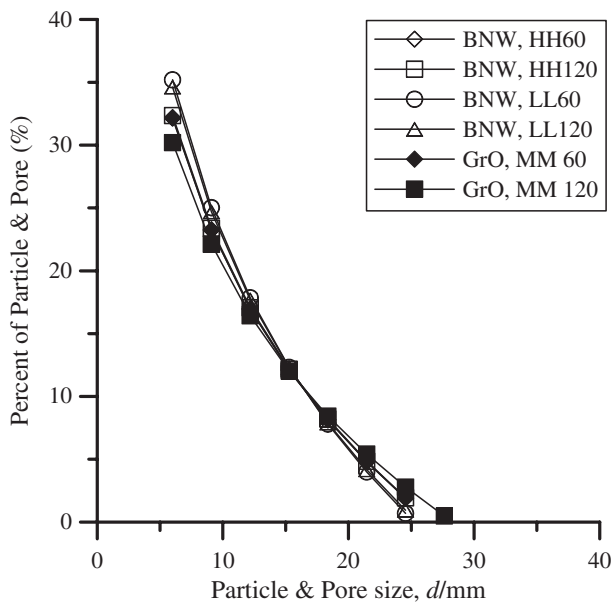


Fig. 5 Population of pores from 5 to 28 μm in size for the six sets of squeeze-cast cakes.

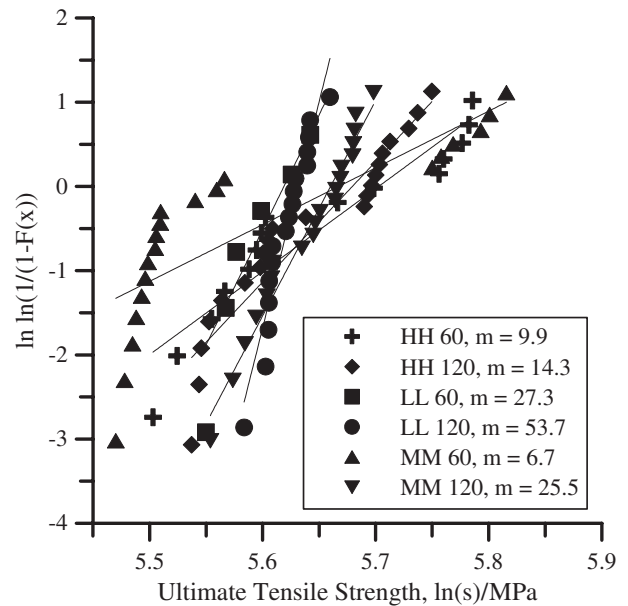


Fig. 6 Weibull modulus of UTS (MPa) for tensile bars prepared from the six sets of forged cakes after T6 treatment.

56.5 counts/mm², 1.64% FRFs, and a Weibull modulus of 25.5. The LL120 samples had 46.8 counts/mm², 0.88% FRFs, and a Weibull modulus of 53.7. A comparison of samples with nearly equal pore counts but different FRFs (LL60: 51.3 counts/mm², 1.13% FRFs; and MM60: 50.7 counts/mm² and 2.21% FRFs) was also made; the former had a Weibull modulus of 27.3, while the latter, a modulus of 6.7.

In this study, we found that the addition of alloying elements to the master A356 alloy led to the generation of a greater area ratio of foggy films than that in the plain A356 ingots. Increasing the Si and Mg contents increased the foggy film area (oxide films) trapped in the chilled samples (5.3%

and 5.8% for the HH alloys versus 3.0% and 4.2% for the LL alloys). Adding Mg to the Al–Si alloy increased the possibility for the formation of surface oxides and entrapment of Mg-bearing inclusions.⁹⁾ The squeezing pressure could fragment the oxide film, thereby greatly decreasing the area ratio of foggy films, while forging could further reduce the amount of oxide film. Since an entrapped oxide film is fragile, cracks can be initiated from within the film, as discussed previously. Therefore, decreasing the size of the oxide film lowers the possibility of crack initiation and propagation, leading to stabilization of the UTS. Interestingly, the Weibull modulus of the forged cakes could be as much as 60 once the pore count decreased to less than



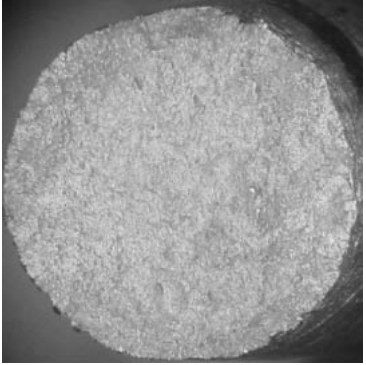
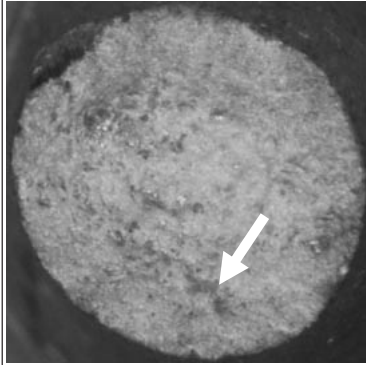
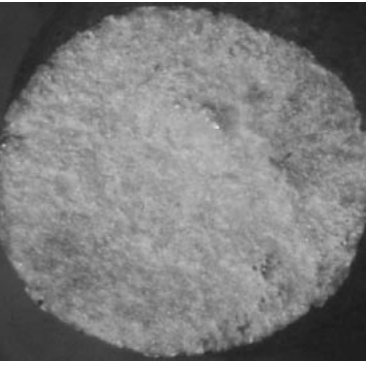
Reaction films (Fracture surface of tensile bars)		
		
BNW lubricant		
	R.F. = 0.28%	R.F. = 0.23%
	a) BNW HH 60	b) BNW LL 60
GrO lubricant		
	R.F. = 1.01%	R.F. = 0.84%
	c) GrO MM 60	d) GrO MM 120

Fig. 7 Records of reaction marks on the fracture surfaces of tensile bars from: (a) HH60 and (b) LL60 samples using lubricant BNW; (c) MM60 and (d) MM 120 samples using lubricant GrO.

45 counts/mm² (5~28 μm) and the FRFs decreased to less than 0.4% (Figs. 8(a) and 8(b)).

3.4 Reaction films observation

The specimens produced using the GrO lubricant exhibited brown and/or black films (or spots) of varying sizes on their fracture surfaces. A possible mechanism for their formation is the decomposition of the lubricant due to the high temperature during pouring, which could have produced gases and possibly bubbles that would have been trapped in the melt during the pouring process. The bubbles would have then collapsed due to the pressure applied during squeezing and would become trapped in the film in the squeeze-cast cakes. Figure 9 shows a film trapped on the fracture surface of a tensile bar (sample MM60). “A” indicates an area on the film, and “B” is nearby a flaky particle. Both indicate the existence of carbon and oxides. “C” marks a location in the matrix that is outside the film. Many particles may also be trapped in the area near the film. Therefore, this film could

presumably be a piece of debris formed by the collapse of a gas bubble. The nearby particles may possibly be reaction products from the collapse of a bubble in the melt, or they could even have been attached to the gas bubble before it collapsed. We also detected the existence of sulfur in the brown reaction film. The decomposition of the oil-based lubricant increased the amount of hydrogen absorbed into the cast, as determined by comparing the samples prepared using the water-based lubricant (0.22~0.3 cc/100 g of Al) with those prepared using the oil-based lubricant (0.31~0.32 cc/100 g of Al) in Table 2.

The oil-based lubricant decomposed due to the high temperature to yield carbon, which was trapped in the melt and could possibly produce aluminum carbide ($4\text{Al} + 3\text{C} \Rightarrow \text{Al}_4\text{C}_3$; $\Delta G_f = -163.16 \text{ kJ/mol}$ at 1000 K^{17}). The black film on the fracture surface was most likely caused due to the existence of aluminum carbide associated with the Gr particles. It is likely that pores would be initiated near the trapped Gr and BN particles via hydrogen diffusion during

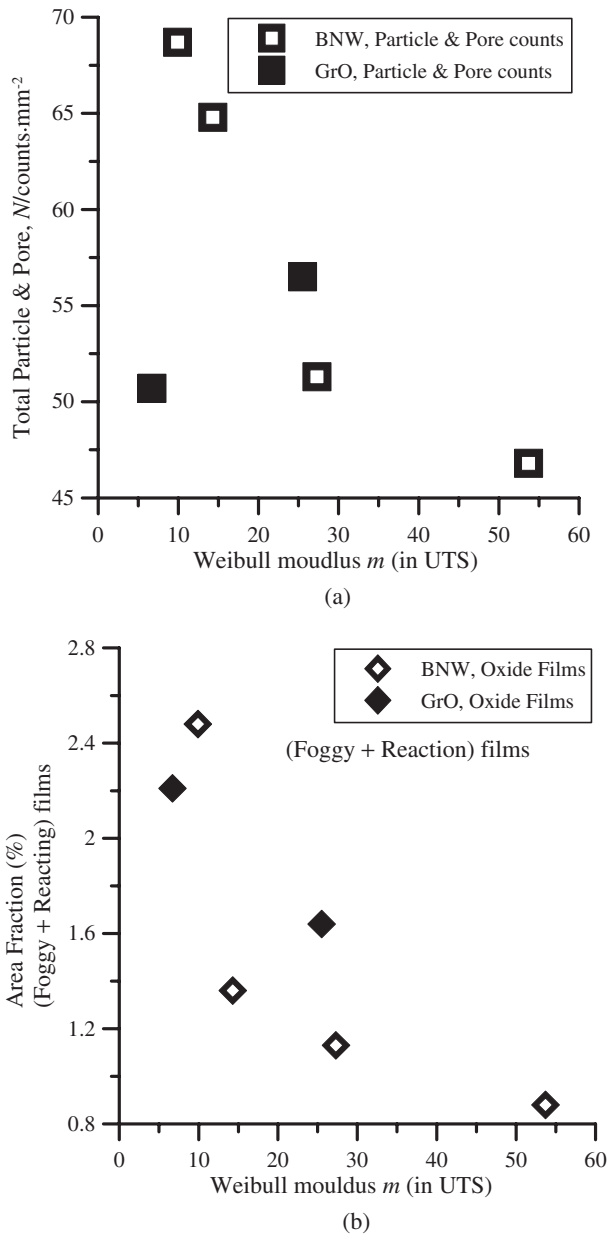


Fig. 8 Relation of (a) the pore counts versus Weibull modulus in UTS and (b) FRFs versus Weibull modulus in UTS for the samples prepared from the six sets of forged cakes after T6 treatment.

solidification as reaction films are often accompanied by pores and/or particles. Therefore, as seen in Table 2, the UTS of the samples produced using the GrO lubricant was considerably deteriorated due to high area ratios of reaction films, even though the melt quality (related pore counts and oxide films) was as good as that of the samples directly prepared from A356 ingots (MM samples).

3.5 Micropore formation

Small pieces of each sample were deep-cooled in liquid nitrogen; these were fractured prior to removal for SEM observation. The arrow in Fig. 10(a) shows a micropore that is 3 μm in size and is located near a trapped particle. Figure 10(b) shows a fine micropore about 1 μm in size on the fracture surface of a specimen produced using the BNW lubricant. These micropores are likely to have originated

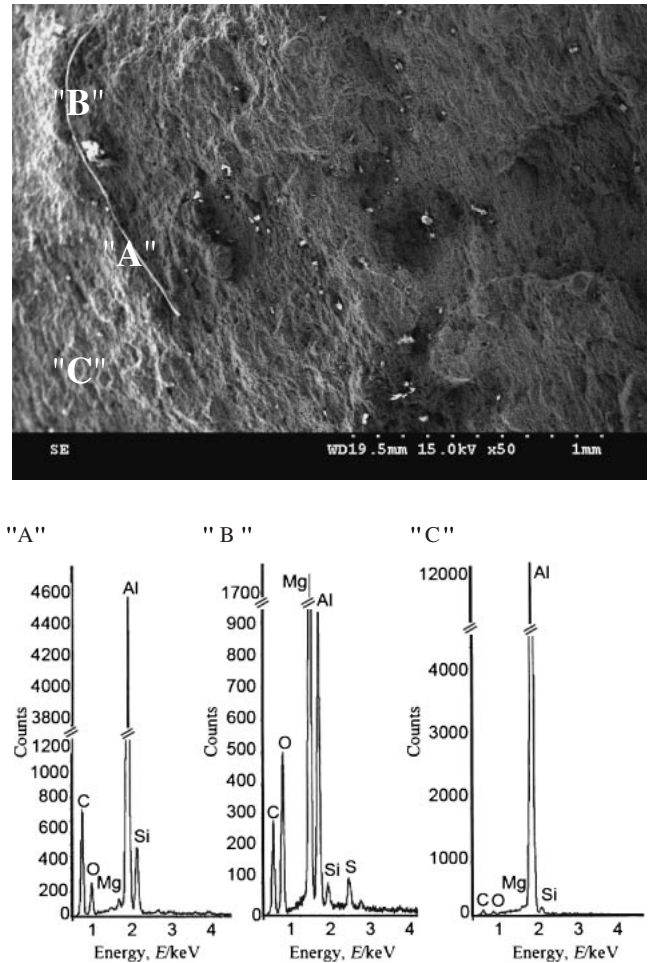


Fig. 9 Scanning electron micrograph showing the fracture surface of a tensile bar produced using GrO, associated with EDAX analyses at "A", "B", and "C".

from degassing. The speed at which a bubble floats is proportional to the square of the radius of the bubble:

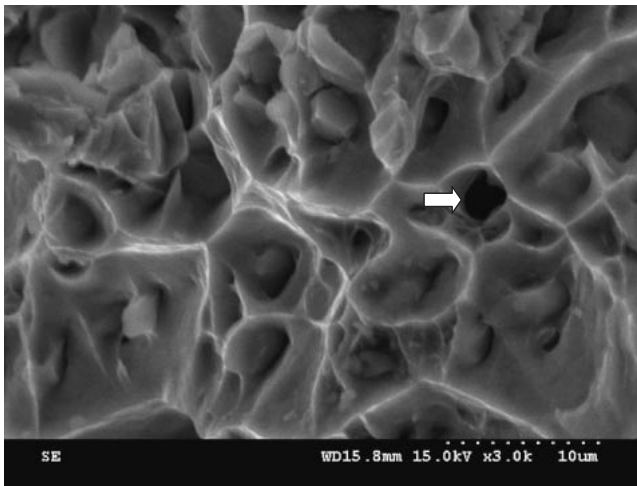
$$V_{st} = 2g(\rho_L - \rho_g)R^2/9\eta, \quad (1)$$

where $g = 9.8 \text{ m/s}^2$, $\rho_L(\text{AL}) = 2.7 \times 10^3 \text{ kg/m}^3$, $\rho_L(\text{H}) = 9 \times 10^{-2} \text{ kg/m}^3$, and $\eta = 1.15 \times 10^6 \text{ Pa}\cdot\text{s}$.^{18,19)} Thus, when the radius of a bubble (R) is equal to 1 μm , its floating speed would be about $5.1 \times 10^{-15} \text{ m/s}$.

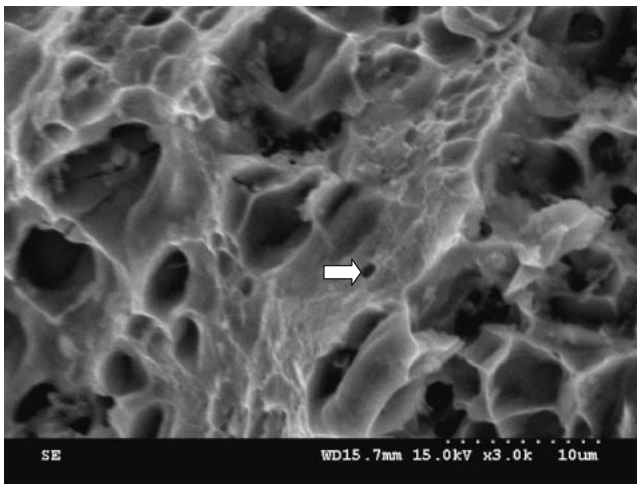
The melt in the crucible was about 400 mm deep, and an induction furnace was used for melting the aluminum alloys. After degassing, microbubbles would likely have moved or floated in the melt throughout the casting process, finally becoming trapped in the casting. The micropores ($<5 \mu\text{m}$) trapped in the matrix would have an effect on the tested tensile properties of the samples; however, this factor is excluded from this discussion since all the six sets of samples were subjected to the same degassing treatment.

4. Conclusion

Among all the variables studied, the Weibull modulus (in UTS) of the Al-6Si-0.3Mg alloy produced using lubricant BNW ($\sim 4 \mu\text{m}$) was the largest (53.7). The pore counts and area ratios of foggy films and reaction films were found to be the key factors influencing the UTS of the tensile specimens



(a)



(b)

Fig. 10 SEM micrograph showing the fracture surfaces of tensile bars (a) produced using from GrO lubricant (the arrow indicates a possible existence of a micropore about 3 μm in size), and (b) produced using from BNW lubricant (the arrow indicates the existence of a micropore about 1 μm in size).

produced from the squeeze-cast cakes after forging and heat-treatment. When the pore count of a cake was less than 47 counts/ mm^2 (5~25 μm in size), the FRFs was less than 0.88%. The squeeze-cast cakes, after forging and T6 treatment, could develop a UTS with a Weibull modulus greater than 53.7.

Acknowledgement

The authors would like to thank the National Science Council of the ROC for their financial support for this study (NSC94-2216-E008-003).

REFERENCES

- 1) G. Lang: *Aluminum* **48** (1972) 664–672.
- 2) J. F. HU and E. N. Pan: *Int. J. Cast. Metals Res.* **10** (1998) 307–319.
- 3) C. R. Loper, Jr.: *AFS Trans.* **100** (1992) 533–538.
- 4) G. E. Negel, J. P. Mourent and J. Dubruel: *AFS Trans.* **91** (1983) 157–160.
- 5) F. A. Fasoyinu: *AFS Trans.* **102** (1994) 515–528.
- 6) Y. Nishida and H. Matsubara: *The British Foundryman* **69** (1976) 274–278.
- 7) I. S. Cho and C. P. Hong: *ISIJ Int.* **37** (1997) 863–871.
- 8) M. Adachi, Y. Waku, H. Iwai, T. Nishi and A. Yoshida: *J. of Japan Institute of Light Metal* **39** (1989) 487–493.
- 9) T. S. Shih and F. S. Shih: *Int. J. Cast. Metals Res.* **10** (1998) 273–282.
- 10) S. M. Lee, H. Shen and C. P. Hong: *ISIJ Int.* **39** (1999) 1160–1168.
- 11) C. P. Hong, H. F. Shen and S. M. Lee: *Metall. Mater. Trans. B-Proc. Metall. Mater. Proc. Sci.* **31B** (2000) 297–305.
- 12) M. Rezvani, X. Yang and J. Campbell: *AFS Trans.* **99-3** (1999) 181–187.
- 13) Y. J. Chen, L. W. Huang and T. S. Shih: *Mater. Trans.* **44** (2003) 327–335.
- 14) Y. J. Chen, L. W. Huang and T. S. Shih: *Mater. Trans.* **44** (2003) 1190–1197.
- 15) L. W. Huang, P. W. Wang, T. S. Shih and J. H. Liou: *Mater. Trans.* **43** (2002) 2913–2920.
- 16) Y. J. Chen and T. S. Shih: *J. of CSME* **23** (2002) 55–67.
- 17) I. Barin: *Thermochemical Data of Pure Substances*, 3rd edition, (Weinheim; New York: VCH, 1995) p. 26.
- 18) A. A. Kulkarni and J. B. Joshi: *Ind. Eng. Chem. Res.* **44** (2005) 5873–5931.
- 19) G. H. Geiger and D. R. Poirier: *Transport Phenomena in Metallurgy*, 2nd edition, (California: Addison-Wesley Publishing Co., 1980) p. 71.